# Type-II-superconductor strip with current in a perpendicular magnetic field

Ernst Helmut Brandt and Mikhail Indenbom*
*Max-Planck-Institut für Metallforschung, Institut für Physik, W-7000 Stuttgart 80, Federal Republic of Germany*
(Received 21 May 1993; revised manuscript received 6 July 1993)

Current density, magnetic field, penetrated magnetic flux, and magnetic moment are calculated analytically for a thin strip of a type-II superconductor carrying a transport current $I$ in a perpendicular magnetic field $H_a$. Constant critical current density $j_c$ is assumed. The exact solutions reveal interesting features of this often realized *perpendicular* geometry that qualitatively differ from the widely used Bean critical state model: At the penetrating flux front the field and current profiles have vertical slopes; the initial penetration depth and penetrated flux are *quadratic* in $H_a$ and $I$; the initial deviation from a linear magnetic moment is *cubic* in $H_a$; the hysteresis losses are proportional to the *fourth* power of a small ac amplitude; the current density $j$ is *finite* over the entire width of the strip even when flux has only partly penetrated; in thin films, as soon as the direction of the temporal change of $H_a$ or $I$ is reversed, $j$ falls below $j_c$ *everywhere*, thus stopping flux creep effectively; the Lorentz force can drive the vortices "uphill" against the flux-density gradient. These analytical results are at variance with the critical-state model for longitudinal geometry and explain numerous experiments in a natural way without the assumption of a surface barrier.

## I. INTRODUCTION

The discovery of high-$T_c$ oxide superconductors[1,2] has revived the interest in experimental methods which measure the electromagnetic properties of these extreme type-II superconductors, namely, irreversible magnetization curves and critical (maximum loss-free) current densities $j_c$,[3,4] nonlinear current-voltage curves and flux creep,[5–7] ac losses and ac susceptibility,[8] and the penetration of magnetic flux by means of magneto-optics.[9–12] Magnetic flux penetrates type-II superconductors in the form of Abrikosov vortices that arrange to a more or less regular flux-line lattice[3,13–15] (FLL) which is pinned by inhomogeneities of the material. If the local current density $j$ exceeds a critical value $j_c$, the flux lines move under the action of a Lorentz force. This flux drift dissipates energy and induces a voltage drop. If the current is driven by an external source (via contacts or inductively) this transport current leads to a stationary dissipative state. If the current is caused by a nonuniform flux-line density $\mathbf{B}(\mathbf{r})$ yielding a current density $\mathbf{j}(\mathbf{r}) = (\partial H/\partial B)\boldsymbol{\nabla} \times \mathbf{B}(\mathbf{r})$ where $H(B) \approx B/\mu_0$ is the reversible magnetic field which is in equilibrium with $B$, then the flux lines rearrange such that $j \leq j_c$ everywhere in the specimen. When this "critical state" is reached, the flux-line motion comes to a halt or "creeps" slowly due to thermally activated depinning[16] or, at low temperatures $T$, due to tunneling of the flux lines out of pins.[17] This "flux creep" is more pronounced in high-$T_c$ superconductors than in conventional superconductors because of the shorter coherence length $\xi$, which means small pinning energy, and because of the higher temperatures of application.[15]

Experiments involving critical currents are often interpreted in terms of the Bean model[3,4,18] that originally applied to long superconductors in a parallel field where demagnetizing effects are negligible. In a Bean critical state, which depends on magnetic history, the current density and flux-density gradient are constant or zero everywhere in the specimen, $j = j_c$ or 0, and $|\boldsymbol{\nabla} B| = \mu_0 j_c$ or 0. Most of the above mentioned experiments, however, use *flat superconductors in a perpendicular field* $H_a$, for example, $c$-axis-oriented monocrystalline platelets or films. In this geometry demagnetizing effects are crucial[3,4,9,19–24] and the Bean model does *not* apply. In particular, the screening currents which shield the specimen's interior from changes of $H_a$, in longitudinal geometry, flow around the specimen only in a surface layer of thickness $\geq \lambda$ ($\lambda$ is the London penetration depth), but in perpendicular geometry the shielding currents flow along the *entire width* of the specimen. Moreover, it is very important that the cross section of real films or flat specimens be *rectangular* rather than ellipsoidal as is often assumed in calculations using a demagnetization factor. The realistic assumption of constant thickness $d$, and thus *constant critical sheet current* $J_c = j_c d$, is one reason why the original Bean results do not apply; see discussion in Sec. VI.

In this paper we show that the current and field profiles in thin type-II superconductors in a perpendicular field $H_a$ or with transport current $I$ qualitatively differ from the original Bean model for longitudinal geometry in many ways.[22–24] The differences listed below are all due to perpendicular geometry but they do not question Bean's main and very useful idea that the flux lines start to move when the current density reaches a critical value $j_c$.

(a) The flux penetration initially is *quadratic* (Bean, linear) in $H_a$ or $I$; i.e., it looks "delayed" as if there were a surface barrier or a large lower critical field $H_{c1}$.

 

(b) The deviation of the magnetic moment from linearity and the remanent moment initially are *cubic* (Bean, quadratic) in $H_a$.

(c) The ac losses initially grow with the *fourth power* (Bean, third) of the amplitude of $H_a$ or $I$.

(d) The penetrating flux front has *vertical* (Bean, constant finite) slope even in the model where a field-independent $j_c$ and vanishing $H_{c1}$ are assumed. In the modified Bean model (with finite $H_{c1}$) the flux front is also vertical but due to completely different reasons.

(e) When the flux has partly penetrated and a critical state with $j = j_c$ is established near the edges of the specimen, the current flows over the *entire width* of the disk or strip in order to shield the central flux-free region (Bean, flux-free region is current free).

(f) The screening current density is a continuous (Bean, piecewise constant) function but has a *vertical slope* at the flux front where it reaches the saturation value $j_c$.

(g) As soon as the direction of the change of $H_a$ or $I$ is reversed, the current density in thin films ($d < \lambda$) falls below $j_c$ *everywhere* (Bean, $j = j_c$); relaxation will therefore stop effectively.

(h) When $H_a$ or $I$ are reversed there appears a spatial region where the driving force on the flux lines acts outwards *against* the pressure of the flux-density gradient (Bean, driving force = flux pressure).

Some of these features were indicated in numerical calculations of the critical state in circular disks,[19–21] but most peculiarities of perpendicular geometry were discovered and proven only by *analytical* calculations in the limit of zero thickness $d$. Such *exact* solutions are available for a current carrying strip[22] and for a disk[23] and strip[24] in a perpendicular field. The present paper compiles and completes these results and extends them to the simultaneous presence of an applied field $H_a$ and transport current $I$ in a strip or flat ring and to arbitrary magnetic history.

For completeness another particular feature of perpendicular geometry shall be mentioned here. In thin superconductors in a perpendicular field the vortex current is predominantly caused by the *curvature* of the magnetic field lines and not by the gradient of the flux density $B = |\mathbf{B}|$. This may be seen by writing $\boldsymbol{\nabla} \times \mathbf{B} = (\boldsymbol{\nabla} B) \times \hat{\mathbf{B}} + B(\boldsymbol{\nabla} \times \hat{\mathbf{B}})$ with $\hat{\mathbf{B}} = \mathbf{B}/B$. Here the first term is the density gradient and the second term the curvature of the field lines. For example, in specimens of half width $a$ and thickness $d$ in a transverse field along $x$, the current density along $z$ is $(\boldsymbol{\nabla} \times \mathbf{H})_z = \partial H_y/\partial x - \partial H_x/\partial y$; in it the first term is related to the curvature radius $\rho = H_x/(\partial H_y/\partial x)$ of the field lines and the second term to the density gradient if the line tilt is small, $|H_y| \ll |H_x|$. In this typical case the curvature term $\partial H_y/\partial x \propto 1/d$ exceeds the gradient term $\partial H_x/\partial y \propto 1/a$ by far. However, if $H_x = 0$ (Meissner state) or if $|H_x| \ll |H_y|$, the field lines are nearly parallel to the surface and the current density is given by the gradient $\partial H_y/\partial x$.

Even a strong curvature of the magnetic *field lines* in current carrying films does not necessarily mean that the *flux lines* (defined by the positions of the vortex core) are also strongly curved. In thin films typically the *flux lines are straight even when transport or shielding currents curve the field lines very strongly.* As shown in Refs. 25 and 26 this has three reasons.

(a) The flux lines have to end perpendicular at the surfaces and thus are straight or sinusoidal with wavelength $d$ in thin films with not too large anisotropy.

(b) The relationship between the shapes of the vortex lines and the magnetic field lines is *nonlocal*; i.e., on short lengths $< \lambda$ the field lines do not have to coincide with the vortex lines.

(c) In thin films with $d < \lambda$ the current is mainly a Meissner surface current even if vortices are present.

The shape of the vortices enters microscopic theories of pinning if the pins are extended along the flux lines, e.g., columnar pins generated by irradiation with heavy ions[27–29] or flat pins such as grain boundaries or twin boundaries.[30–32] These microscopic details do not enter the macroscopic considerations presented below.

In order to visualize the essential features of perpendicular geometry and to facilitate the correct interpretation of experimental data, the present paper gives explicit analytical solutions for a thin superconducting strip carrying a transport current $I$ along $-z$ and shielding an applied perpendicular magnetic field $H_a$ along $x$. The critical current density $j_c$ is assumed to be constant, i.e., independent of the local flux density. The strip fills the space $|x| \le d/2$, $|y| \le a$, $|z| < \infty$ with $a \gg d$. The main quantity we calculate is the current density (along $-z$) integrated over the specimen thickness, $J(y) = \int_{-d/2}^{d/2} j(x,y)\,dx$ (sheet current, in units A/m like $H_a$). For the present purpose it is *irrelevant* whether this is a Meissner current or vortex current or both; i.e., $d < \lambda$ or $d > \lambda$ are allowed as long as $d \ll a$. Since only the *integrated* current enters and we are interested in a spatial resolution $> d$ along $y$, the current distribution along $x$ does not matter, and the only assumption for the presented calculations is $d \ll a$. The thickness $d$ should be finite since $J$ should be finite. Obviously, in the completely flux-free region the current is a pure Meissner current

$$j(x,y) = J(y)\,\cosh(x/\lambda)/[\,2\lambda \sinh(d/2\lambda)\,]\,,$$

which, for $d \gg \lambda$, flows in two surface layers of thickness $\lambda$ leaving the central region current free. As soon as the flux penetrates, the current density is limited to $j_c$ since for $|j| > j_c$ the flux lines move and rearrange such that $|j| \le j_c$ holds everywhere.

From the sheet current $J(y)$ (along $-z$) the magnetic field $\mathbf{H}(x,y) = \mathbf{B}(x,y)/\mu_0$ is obtained by Ampère's law. To an accuracy of $d/a$, the field $\mathbf{H}$ at the specimen surfaces has the parallel components $H_y(d/2,y) = -\frac{1}{2}J(y)$ (upper surface) and $H_y(-d/2,y) = \frac{1}{2}J(y)$ (lower surface) and the perpendicular component $H_x(d/2,y) = H_x(-d/2,y) = H(y)$ with

$$H(y) = \frac{1}{2\pi}\int_{-a}^{a} \frac{J(u)\,du}{y-u} + H_a. \tag{1.1}$$

Both components in whole space outside the conductor follow from

$$\mathbf{H}(x,y)=\frac{1}{2\pi}\int_{-a}^{a}\frac{(y-u,-x)\,J(u)}{(y-u)^2+x^2}du+\mathbf{H}_a,$$

since $x/(u^2+x^2)\approx\pi\,\delta(u)\,\mathrm{sgn}(x)$ for $x\to 0$.

The negative magnetic moment $M$ and the total magnetic flux $\Phi$ per unit length of the strip are defined by

$$M=\int_{-a}^{a}y\,J(y)\,dy\ , \tag{1.2}$$

$$\mu_0^{-1}\Phi=\int_{-a}^{a}H(y)\,dy$$
$$=2aH_a+\frac{1}{2\pi}\int_{-a}^{a}J(u)\,\ln\left|\frac{a-u}{a+u}\right|du. \tag{1.3}$$

Interestingly, only one-half of the total magnetic moment $\mathbf{m}=\frac{1}{2}\int\mathbf{r}\times\mathbf{j}\,d^3r$ comes from the currents $J(y)$ flowing *along* the strip. The other half originates from the transverse currents (along $\pm\hat{y}$) which occur at the far-away ends of the strip where the currents perform a U turn. Both contributions are proportional to the strip length $L\gg a$ and are exactly equal since $\mathbf{j}=0$. This fact allows one to express $M=-m_x/L$ in terms of $j_z$ only. The resulting moment, Eq. (1.2), therefore, no longer contains the factor 1/2 of the original definition.

Equation (1.1) may be inverted to give[33]

$$J(y)=\frac{2}{\pi}\int_{-a}^{a}\frac{H_x(u)-H_a}{y-u}\left(\frac{a^2-u^2}{a^2-y^2}\right)^{1/2}du$$
$$+I/[\pi(a^2-y^2)^{1/2}]\ , \tag{1.4}$$

where $I=\int_{-a}^{a}J(y)\,dy$ is the total current through the strip. This result is obtained by conformal mapping of the strip cross section onto a circle as shown, e.g., in Refs. 22 and 34. The first term in (1.4) originates from the shielding current induced by an applied field or by magnetic poles of strength $H_x(y)-H_a$ on the surface of the circle, and the second term comes from a constant current in the circle of conformal mapping. Note that a constant current along a cylinder of circular cross section does not generate a magnetic field inside the cylinder and thus does not influence the shielding; mapping back then yields $J(y)\sim(a^2-y^2)^{-1/2}$.

A general method that inverts Ampère's law for thin flat conductors or superconductors of arbitrary shape and determines the current distribution $\mathbf{J}(y,z)$ from the measured perpendicular surface field $H_x(y,z)$ is given in Ref. 33.

## II. STRIP WITH TRANSPORT CURRENT

As long as the strip is in the Meissner state, no magnetic flux has penetrated; thus $H(y)=0$, for $-a\le y\le a$. The perpendicular components of an applied field $H_a$ and of the field caused by an applied current $I$ are then completely shielded from the strip by appropriate screening currents $J(y)$, even if $d<\lambda$, as long as $a\gg 2\lambda^2/d$. For the case $H_a=0$, $I\neq 0$, one gets from (1.4) the classical formula[35]

$$J_{\rm ideal}(y)=I/[\pi(a^2-y^2)^{1/2}]\ , \tag{2.1}$$

which inserted in (1.1) gives inside the strip $H(|y|<a)=0$ and outside

$$H_{\rm ideal}(|y|>a)=\frac{I}{2\pi}\frac{y/|y|}{(y^2-a^2)^{1/2}}. \tag{2.2}$$

The field (2.2) has the expected far-field behavior $H(|y|\gg a)=I/(2\pi y)$ and at the specimen edges exhibits a square-root infinity $H\propto(|y|-a)^{-1/2}$ as does the current density $J\propto(|y|-a)^{-1/2}$. As a consequence of these infinities, flux starts to penetrate at the edges and the sheet current $J(y)$ is limited to the critical value $J_c=j_cd$ near the edges. Here enters our realistic assumption of constant thickness $d(y)=d=$const. For a nonrectangular (say, elliptical) cross section the critical sheet current depends on $y$, $J_c(y)=j_cd(y)$, and the results derived in this paper do not apply. The generalization to arbitrary $J_c(y)$ is obvious from the following derivation.

As stated above, our calculations do not require any knowledge about the current distribution $j(x,y)$ across the specimen thickness $d$ (along $x$). It suffices to know that the integral sheet current $|J|$ is limited to the value $J_c$. However, to fix ideas, we briefly discuss the current penetration along $x$. There are two limiting cases.

(a) If $d<\lambda$ and $J<2\tilde{H}_{c1}$ [$\tilde{H}_{c1}\approx(\lambda/d)H_{c1}=$ effective $H_{c1}$ of films in longitudinal field], the current is mainly a Meissner surface current, which is independent of the vortex positions and vortex curvature and is nearly uniform, $j(x,y)\approx J(y)/d$. As shown in Refs. 25 and 26, if $d\ll\lambda$, the vortex lines will be straight and perpendicular to the film even when the magnetic field lines inside the superconductor are strongly *curved* due to the presence of a large current density, or *tilted* due to a tilted applied field.

(b) If $d\gg\lambda$, the current is a Meissner current only in the region where no parallel or perpendicular magnetic flux has penetrated. Else, for $J>2H_{c1}$, the flux and current penetration along $x$ is described in the usual way by the well-known Bean model for longitudinal geometry. This penetration along the *perpendicular* coordinate $x$ is *not* the subject of this paper, which deals with the penetration of current and perpendicular flux along the *parallel* coordinate $y$ into a strip which has edges and in which the sheet current is limited to $J_c$. The *current-induced* Bean critical state across the thickness of our strip occurs for $d\gg\lambda$, *irrespective* of whether $J(y)$ is a transport current (Sec. II), an induced current (Sec. III), or both (Sec. IV). In this classical Bean critical state along $x$, one has $j(x,y)=\pm j_c$ or 0, and thus $J(y)=(h_+-h_-)j_c$ where $h_+$ and $h_-$ are the (history dependent) integral thicknesses of the regions carrying $+j_c$ or $-j_c$, respectively ($h_++h_-\le d$).

The dissipation connected with this irreversible penetration of $j(x,y)$ along $x$ is negligibly small compared to that of the penetration along $y$, since the path along $x$ is much shorter ($\le d$) than the path the vortex lines move along $y$.

The problem of current saturation in a thin strip was solved by Norris[22] by conformal mapping. Flux penetrates from the edges such that $H(y)=0$ for $|y|\le b$, $|J(y)|<J_c$ for $|y|<b$ (shielding currents), and $|J(y)|=$

$J_c$ for $b < |y| < a$. One first has to find the currents $J(y, y_0)$ which flow in the region $|y| < b$ and shield there the field caused by a current of unit strength flowing along a line at $y = y_0 > b$. Conformal mapping yields

$$J(y, y_0) = (y_0^2 - b^2)^{1/2}/[2\pi(y_0 - y)(b^2 - y^2)^{1/2}]. \quad (2.3)$$

From (2.3) the shielding currents which in $|y| < b$ compensate the field caused by a constant current density $J_c$ flowing in the strips $-a \le y \le -b$ and $b \le y \le a$ are obtained by integrating $J(y, y_0) + J(y, -y_0)$ over the interval $b \le y_0 \le a$. To this integral one has to add a contribution $\propto (b^2 - y^2)^{-1/2}$ [cf. $J_{\rm ideal}$ (2.1)] such that the infinities at $y = \pm b$ compensate each other. The final result is (Fig. 1)

$$J(y) = \begin{cases} \dfrac{2J_c}{\pi} \arctan\left(\dfrac{a^2 - b^2}{b^2 - y^2}\right)^{1/2}, & |y| < b \\ J_c, & b < |y| < a. \end{cases} \quad (2.4)$$

Integrating this one gets the total current

$$I = 2J_c\,(a^2 - b^2)^{1/2}, \quad b = a(1 - I^2/I_{\rm max}^2)^{1/2}\,, \quad (2.5)$$

where $I_{\rm max} = 2aJ_c$ is the maximum total current occurring at full penetration $b = 0$. Inserting (2.4) into (1.1) we obtain the magnetic field component perpendicular to the strip,

$$H(y) = \begin{cases} 0, & |y| < b \\ \dfrac{H_c y}{|y|} \operatorname{arctanh}\left[\dfrac{y^2 - b^2}{a^2 - b^2}\right]^{1/2}, & b < |y| < a \\ \dfrac{H_c y}{|y|} \operatorname{arctanh}\left[\dfrac{a^2 - b^2}{y^2 - b^2}\right]^{1/2}, & |y| > a\,, \end{cases} \quad (2.6)$$

with $H_c = J_c/\pi$. The distinction of the cases $|y| > a$ and $|y| < a$ in (2.6) may be avoided by writing $\arctan x$ and $\arctan(1/x)$ in the same form $(1/2)\ln|(1 + x)/(1 - x)|$. Near the strip edges one has now a *logarithmic* singularity

$$H(y) = \frac{H_c}{2}\frac{y}{|y|} \ln\frac{2(a^2 - b^2)}{|\,|y| - a\,|\,a}, \qquad |y| \approx a\,.$$

The magnetic moment $M$ and total flux $\Phi$ of the current carrying strip are zero due to symmetry. The flux through the half strip is

$$\Phi_h = \mu_0 H_c \left[(a^2 - b^2)^{1/2} \operatorname{arccosh}\frac{a}{b} - a \ln\frac{a}{b}\right]$$
$$= \frac{\mu_0 H_c a}{2}[(1 + x)\ln(1 + x) + (1 - x)\ln(1 - x)]\,, \quad (2.7)$$

with $x = I/I_{\rm max}$. For *weak penetration* $a - b \ll a$ one obtains from (2.5)–(2.7) $a - b \approx ax^2/2$, $\Phi_h \approx \mu_0 H_c a x^2/2$, or

$$a - b \approx aI^2/2I_{\rm max}^2, \quad \Phi_h \approx (a - b)\mu_0 H_c \propto I^2. \quad (2.8)$$

For *complete penetration* $b = 0$ one has $\Phi_h = a\mu_0 H_c \ln 2$. The current density and the field have *vertical slopes* at $|y| = b$. Near $|y| = b$ one has

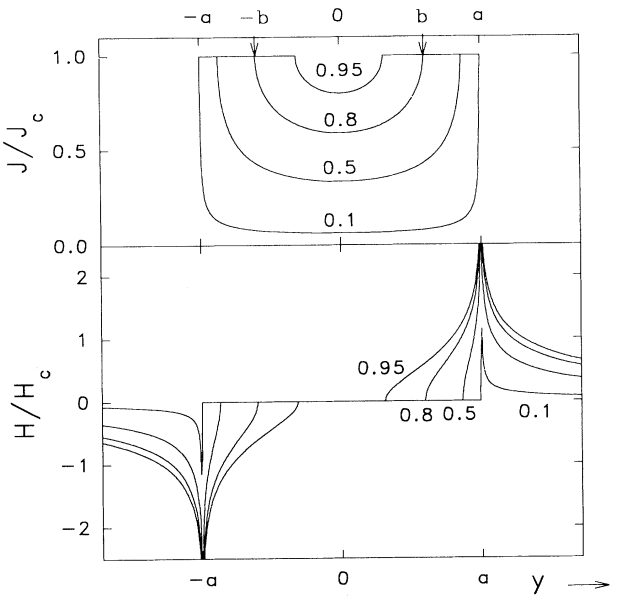


FIG. 1. Current density $J(y)$ (2.4) (top) and magnetic field $H(y)$ (2.6) (bottom) in a superconducting strip of width $2a$ carrying a transport current $I$ which is increased from zero (virgin state). The depicted profiles are for $I/I_{\rm max} = 0.1$, 0.5, 0.8, and 0.95. For $I/I_{\rm max} = 0.8$ the penetration width $b$ is indicated at the top.

$$J(y) = J_c - J_c\frac{2}{\pi}\left(\frac{b^2 - y^2}{a^2 - b^2}\right)^{1/2}, \quad |y| < b\,, \quad (2.9)$$

$$H(y) = H_c\left(\frac{y^2 - b^2}{a^2 - b^2}\right)^{1/2}, \quad |y| > b. \quad (2.10)$$

For $b < a/2$ or $I/I_{\rm max} > 0.7$, the elliptical dip (2.9) in $J(y)$ is a good approximation for all $|y| \le b$.

The results (2.4)–(2.10) apply to the virgin state where $I$ is increased from zero. The corresponding expressions for alternating applied current with amplitude $I_0$ are obtained by looking, e.g., at the situation when $I$ is decreased monotonically from $I_0$ to $-I_0$. One easily shows that the resulting current and field profiles $J_\downarrow$ and $H_\downarrow$ are linear superpositions of the form (Fig. 2)

$$J_\downarrow(y, I, J_c) = J(y, I_0, J_c) - J(y, I_0 - I, 2J_c)\,, \quad (2.11)$$
$$H_\downarrow(y, I, J_c) = H(y, I_0, J_c) - H(y, I_0 - I, 2J_c)\,, \quad (2.12)$$

with $J(y, I, J_c)$ and $H(y, I, J_c)$ given by (2.4) and (2.6) with $b$ from (2.5). At intermediate applied currents $-I_0 < I < I_0$ there is a new penetration width $b' = a[1 - (I \pm I_0)^2/4I_{\rm max}^2]$ inside which $H(y)$ is frozen like in the Bean model though $J(y)$ changes *everywhere*, with the vertical slope at $|y| = b = a(1 - I^2/I_{\rm max}^2)^{1/2}$ persisting and a new saturation to $J(y) = -J_c$ occurring at $|y| > b'$.

When $I = -I_0$ is reached, the original virgin state is reestablished, with $J$ and $H$ having changed sign, $J(y, -I_0, J_c) = -J(y, I_0, J_c)$ and $H(y, -I_0, J_c) = -H(y, I_0, J_c)$. In the half period with *increasing* $I$ one

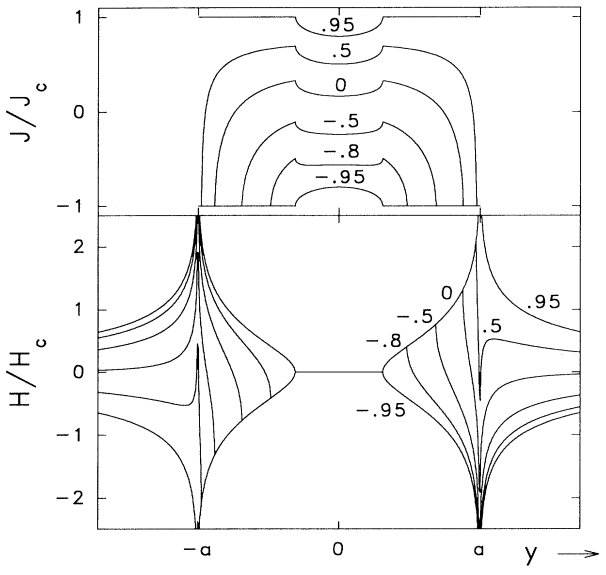


FIG. 2. Current density $J_\downarrow(y)$ (2.11) (top) and magnetic field $H_\downarrow(y)$ (2.12) (bottom) in a superconducting strip of width $2a$ when the transport current $I$ is reduced from $0.95I_{\max}$ to $-0.95I_{\max}$. Shown are the profiles for $I/I_{\max} = 0.95, 0.5, 0, -0.5, -0.8, -0.95$.

has $J_\uparrow(y,I,J_c) = -J_\downarrow(y,-I,J_c)$ and $H_\uparrow(y,I,J_c) = -H_\downarrow(y,-I,J_c)$. For general magnetic history $I(t)$ ($t$ = time) the current and field profiles of the strip are described by similar superpositions as (2.11) and (2.12) depending on $I(t)$ and on all previously reached maxima of $|I(t)|$ in such a way that each maximum erases the memory of all previously reached smaller maxima. The virgin solution (2.4)–(2.6), therefore, completely determines any possible critical state of a current carrying strip in zero field.

The hysteretic losses caused in the strip by an alternating current $I(t)$ with amplitude $I_0$ and frequency $\nu$ were calculated by Norris.[22] When $I$ increases from $-I_0$ to $I_0$ the electric field in the strip is $E(y) = \partial\Phi(y)/\partial t$ with flux $\Phi(y) = \mu_0 \int_0^y H(u)\,du$. The energy dissipated in the strip during this half cycle is then

$$U_{\rm HC} = \int dt \int_{-a}^{a} E(y)J(y)\,dy = 2\mu_0 J_c \int_b^a dy \int_b^y H(u)\,du\ , \tag{2.13}$$

since $H(|y|<b) = 0$ and $J(|y|>b) = J_c$. In (2.13) $H(y)$ has to be taken at the current maximum $I = I_0$. The hysteretic ac losses are thus uniquely determined by the field profile at peak current. Inserting (2.6) in (2.13) and performing the integrals one obtains the dissipated power $P = 2\nu U_{\rm HC}$ per unit length of the strip,[22]

$$P = (\nu\mu_0 I_{\max}^2/\pi)\, f(I_0/I_{\max})\ , \tag{2.14}$$

$$f(x) = (1-x)\ln(1-x) + (1+x)\ln(1+x) - x^2\ .$$

For small and large amplitudes this gives

$$P = (\nu\mu_0/6\pi I_{\max}^2)\, I_0^4, \qquad I_0 \ll I_{\max}\ , \tag{2.15}$$

$$P = (\nu\mu_0/\pi)\,(2\ln 2 - 1)\, I_{\max}^2, \qquad I_0 = I_{\max}. \tag{2.16}$$

The initial losses are thus very small, $P \sim I_0^4$. More features of this solution are discussed in Sec. VI.

## III. STRIP IN A PERPENDICULAR FIELD

The current and field profiles in a thin strip in a perpendicular field $H_a$ and with zero transport current $I$ can be calculated in a similar way as for the current carrying strip in Sec. I. Moreover, the current-induced Bean critical state in the $x$ direction is *the same* as in Sec. II. In the ideal Meissner state one has $H(|y|<a) = 0$ and from (1.1), (1.2), (1.4),[35,36]

$$J_{\rm ideal}(y) = 2yH_a/(a^2-y^2)^{1/2}\ , \tag{3.1}$$

$$H_{\rm ideal}(|y|>a) = |y|H_a/(y^2-a^2)^{1/2}\ , \tag{3.2}$$

$$M_{\rm ideal} = \pi a^2 H_a. \tag{3.3}$$

The current through the half width is $I_h = 2aH_a$.

The saturation of $|J(y)| = J_c$ in the region $b \le |y| \le a$ is accounted for by integrating $J(y,y_0) - J(y,-y_0)$, Eq. (2.3), over $b \le y_0 \le a$ and adding the shielding currents caused in the flux-free region $|y| \le b$ by the applied field $H_a$. This gives for $|y| \le b$

$$J(y) = \frac{2yJ_c/\pi}{(b^2-y^2)^{1/2}}\left[\int_b^a \frac{(u^2-b^2)^{1/2}}{u^2-y^2}\,du - \frac{\pi H_a}{J_c}\right]. \tag{3.4}$$

The integral in (3.4) may be performed by substituting $z = (u^2-b^2)^{1/2}$, yielding a term vanishing at $|y| = b$ and a constant term. This constant term has to compensate the term $-\pi H_a/J_c$; otherwise $J(y)$ would have an unphysical infinity at $y = b$ caused by the factor in front of the brackets. This condition fixes $b$,

$$b = a/\cosh(H_a/H_c)\ , \tag{3.5}$$

$$c \equiv (a^2-b^2)^{1/2}/a = \tanh(H_a/H_c)\ , \tag{3.6}$$

where $H_c = J_c/\pi$ and $c$ is a constant needed below. The resulting current and negative magnetic moment in this virgin state (for $H_a$ increased from zero) are (Fig. 3)

$$J(y) = \begin{cases} \dfrac{2J_c}{\pi}\arctan\dfrac{cy}{(b^2-y^2)^{1/2}}, & |y|<b \\ J_c\, y/|y|, & b<|y|<a\ , \end{cases} \tag{3.7}$$

$$M = J_c a^2 c = J_c a^2 \tanh(H_a/H_c). \tag{3.8}$$

From (1.1) and (3.7) the field and the penetrated flux are

$$H(y) = \begin{cases} 0, & |y|<b \\ H_c\,\mathrm{arctanh}\dfrac{(y^2-b^2)^{1/2}}{c\,|y|}, & b<|y|<a \\ H_c\,\mathrm{arctanh}\dfrac{c\,|y|}{(y^2-b^2)^{1/2}}, & |y|>a\ , \end{cases} \tag{3.9}$$

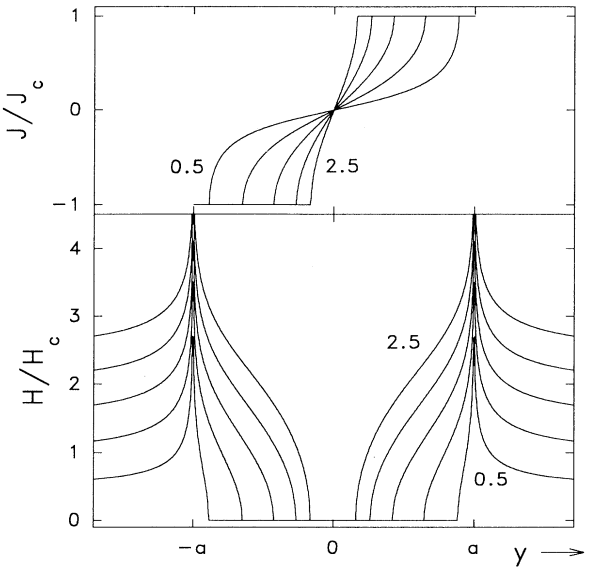


FIG. 3. Current density $J(y)$ (3.7) (top) and magnetic field $H(y)$ (3.9) (bottom) in a superconducting strip of width $2a$ in a perpendicular magnetic field $H_a$ which is increased from zero (virgin state). The depicted profiles are for $H_a/H_c = 0.5, 1, 1.5, 2, 2.5$.

$$\Phi = 2\mu_0 H_c a \ln\frac{a}{b} = 2\mu_0 H_c a \ln\cosh\frac{H_a}{H_c}. \tag{3.10}$$

As in the current carrying strip, the current density and the flux front at $|y| = b$ have vertical slopes, $|J(y)| - J_c \sim H(y) \sim (|y| - b)^{1/2}$, and the infinity at the edges is logarithmic,

$$H(y) \approx \frac{H_c}{2} \ln\frac{2a(a^2 - b^2)}{||y| - a|\, b^2}, \qquad |y| \approx a\ .$$

The analytical solution $H(y)$ (3.9) thus proves a *vertical slope of the penetrating flux front* for our model, in which $J_c = \text{const}$ and a lower critical field $H_{c1} = 0$ were assumed. Interestingly, the fact that the reversible magnetization curve exhibits $\partial H/\partial B = 0$ at $H = H_{c1}$ or $B = 0$ leads *also* to a vertical slope of the flux profile at the flux front, even in *longitudinal* geometry, since the current density $\mathbf{j} = (\partial H/\partial B)\nabla \times \mathbf{B}$ and Lorentz force density $\mathbf{j} \times \mathbf{B}$ contain this vanishing factor; therefore, if $j$ is balanced by a constant $j_c$ the factor $\nabla \times \mathbf{B}$ has to become infinitely large when $B$ goes to zero. Note that the vertical slopes in this modified Bean model ($H_{c1} \neq 0$) in longitudinal geometry, and the vertical slope in the simple Bean model ($H_{c1} = 0$) in perpendicular geometry, have *completely different physical reasons.*

In the limit $J_c \to \infty$ (3.5)–(3.9) reproduce the ideal-shielding results (3.1)–(3.3). For *weak penetration* ($H_a \ll H_c$) one gets from (3.5)–(3.10)

$$b = a - aH_a^2/2H_c^2\ , \tag{3.11}$$
$$M = \pi a^2 H_a(1 - H_a^2/3H_c^2)\ , \tag{3.12}$$
$$\Phi = \mu_0 a H_a^2/H_c. \tag{3.13}$$

For *almost complete penetration* ($H_a \gg H_c$) one gets

$$b = 2a\exp(-H_a/H_c) \ll a\ , \tag{3.14}$$
$$M = J_c a^2[1 - 2\exp(-2H_a/H_c)]\ , \tag{3.15}$$
$$J(|y| < b) = (2J_c/\pi)\arcsin(y/b)\ , \tag{3.16}$$
$$H(b < |y| < a/2) = H_c\,\text{arccosh}|y/b|\ , \tag{3.17}$$
$$H(2b < |y| < \infty) = H_a + H_c \ln|a^2/y^2 - 1|^{-1/2}\ , \tag{3.18}$$
$$\Phi = 2\mu_0 a(H_a - 0.69H_c). \tag{3.19}$$

Very recently the current density of a type-II superconducting circular disk in perpendicular field was calculated analytically.[23] Comparison with the above results reveals that the penetration width (3.5) and current distribution (3.7) exhibit the same functional dependences for the strip and the disk if one replaces $y/a$ by $r/R$, $J$ by $2J/\pi$, and $J_c$ by $2J_c/\pi$. The same replacement works also for the current (3.20) below. The magnetization (3.8) and field (3.9) (obtained for the disk numerically in Ref. 23) are, however, different in both geometries.

When the applied field $H_a$ oscillates between the extremal values $\pm H_0$ with frequency $\nu$, it suffices to consider one half period, say, decreasing $H_a$. Similarly as for the oscillating applied current in Sec. II, one can show that for $H_a$ decreasing from $+H_0$ to $-H_0$ the current distribution $J_\downarrow$, field $H_\downarrow$, negative magnetic moment $M_\downarrow$, and flux $\Phi_\downarrow$ follow from the "virgin" results (3.6)–(3.10) by linear superpositions of the form (Fig. 4)

$$J_\downarrow(y, H_a, J_c) = J(y, H_0, J_c) - J(y, H_0 - H_a, 2J_c)\ , \tag{3.20}$$
$$H_\downarrow(y, H_a, J_c) = H(y, H_0, J_c) - H(y, H_0 - H_a, 2J_c)\ , \tag{3.21}$$
$$M_\downarrow(H_a, J_c) = M(H_0, J_c) - M(H_0 - H_a, 2J_c)\ , \tag{3.22}$$
$$\Phi_\downarrow(H_a, J_c) = \Phi(H_0, J_c) - \Phi(H_0 - H_a, 2J_c). \tag{3.23}$$

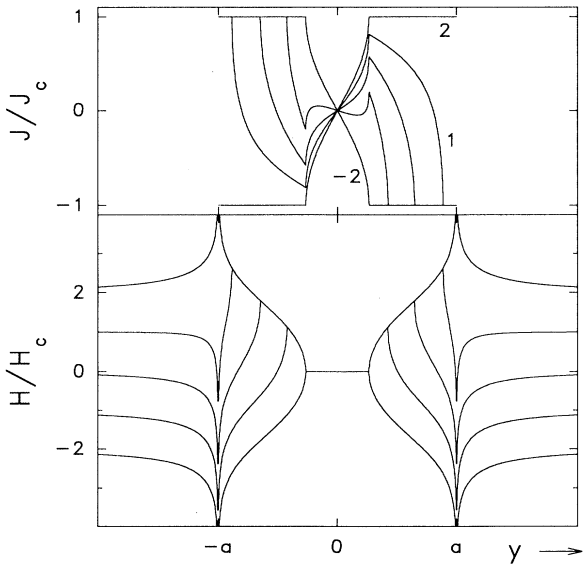


FIG. 4. Current density $J_\downarrow(y)$ (3.20) (top) and magnetic field $H_\downarrow(y)$ (3.21) (bottom) in a superconducting strip of width $2a$ when the applied field $H_a$ is reduced from $2H_c$ to $-2H_c$. Shown are the profiles for $H_a/H_c = 2, 1, 0, -1, -2$.

At $H_a = -H_0$ the original virgin state is reached again; $J$, $H$, $M$, and $\Phi$ have just changed sign. In the half period with increasing $H_a$ one has $J_\uparrow(y, H_a, J_c) = -J_\downarrow(y, -H_a, J_c)$, $H_\uparrow(y, H_a, J_c) = -H_\downarrow(y, -H_a, J_c)$, $M_\uparrow(H_a, J_c) = -M_\downarrow(-H_a, J_c)$, and $\Phi_\uparrow(H_a, J_c) = -\Phi_\downarrow(-H_a, J_c)$. At intermediate fields $|H_a| < H_0$ there is a new penetration width $b' = a/\cosh(|H_0 \pm H_a|/2H_c)$ inside which $H$ is frozen like in the Bean model though $J$ changes *everywhere*; the vertical slope of $J(y)$ at $|y| = b = a/\cosh(H_0/H_c)$ remains visible and new saturation occurs at $|y| > b'$.

For *general* magnetic history $H_a(t)$ ($t$ = time) the critical state of the strip is described by a similar superposition as (3.20)–(3.23) which now depends on $H_a(t)$ and on all previously reached maximum values of $|H_a(t)|$ such that each maximum wipes out the memory of all previous smaller maxima. Thus, the solution (3.5)–(3.10) *completely determines any possible critical state in the strip.*

When $H_a$ oscillates with frequency $\nu$ and amplitude $H_0$ the negative magnetic moment cycles the hysteretic magnetization curve (Fig. 5)

$$M_{\downarrow\uparrow} = \pm J_c a^2 \left[\tanh\frac{H_0}{H_c} + 2\tanh\frac{H_a \mp H_0}{2H_c}\right]. \tag{3.24}$$

The remanent negative magnetic moment observed after $H_a$ is decreased to zero from the virgin state is (Fig. 5)

$$M_{\rm rem}(H_0) = J_c a^2 \left[\tanh\frac{H_0}{H_c} - 2\tanh\frac{H_0}{2H_c}\right]. \tag{3.25}$$

The hysteresis losses $P(H_0)$ are frequency times area of the hysteresis loop,

$$P = \nu\mu_0 \oint M(H_a)\, dH_a = 4\nu\mu_0 a^2 J_c H_0\, g\left(\frac{H_0}{H_c}\right), \tag{3.26}$$

$$g(x) = (2/x)\ln\cosh x - \tanh x.$$

For small and large amplitude $H_0$ this gives

$$P = (2\pi\nu\mu_0 a^2/3H_c^2)\, H_0^4, \qquad H_0 \ll H_c a\,, \tag{3.27}$$

$$P = 4\nu\mu_0 a^2 J_c\,(H_0 - 1.386 H_c), \qquad H_0 \gg H_c. \tag{3.28}$$

The energy loss is thus initially very small, $P \sim H_0^4$. For further discussion of flux penetration see Sec. VI.

## IV. CURRENT CARRYING STRIP IN A PERPENDICULAR FIELD

When both a transport current $I$ and a magnetic field $H_a$ are applied to a thin strip with constant $J_c$, a rich variety of qualitatively different current and field profiles occur depending on the history of $I(t)$ and $H_a(t)$. We shall visualize this by considering the special case where $I$ and $H_a$ are increased from zero simultaneously. This situation with constant $I(t)/H_a$ is realized, e.g., when a perpendicular field is applied to a flat superconducting ring or to a closed double strip as discussed in Sec. V.

The general solution to this nonlinear problem can be constructed from the "current only" and "field only" solutions obtained in Secs. II and III. We denote these by $J_I(y)$, $H_I(y)$, and $J_H(y)$, $H_H(y)$, respectively. Obviously, by adding these even and odd solutions with weight 1/2 each, we obtain a "current density" $J^*(y) = (J_I + J_H)/2$ which exhibits $J^*(b < y < a) = J_c$, $J^*(-\infty < y < -b) = 0$, and a flux-free region $-b < y < b$ (Fig. 6). Note that the auxiliary function $J^*(y)$ is formally defined as zero also in the intervall $-\infty < y \le -a$ outside the strip, where the physical current densities $J_I$ (2.4) and $J_H$ (3.7) are not defined. This property will be required for superpositions constructed below.

We write this solution as

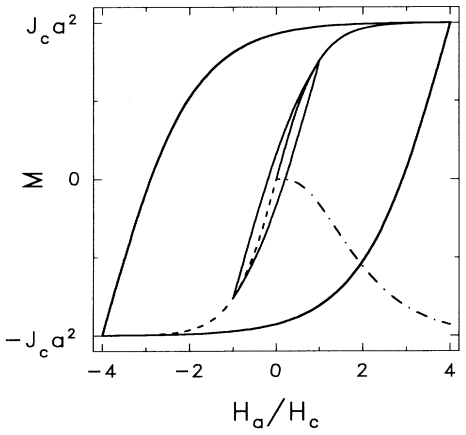


FIG. 5. The negative magnetic moment $M_{\downarrow\uparrow}(H_a)$ (3.24) per unit length of the strip in a perpendicular magnetic field $H_a$ which is cycled with amplitudes $H_0 = 4H_c$ and $H_0 = H_c$. The dashed and solid curves through the origin are the virgin curves (3.8). The dash-dotted curve gives the negative remanent moment (3.25).

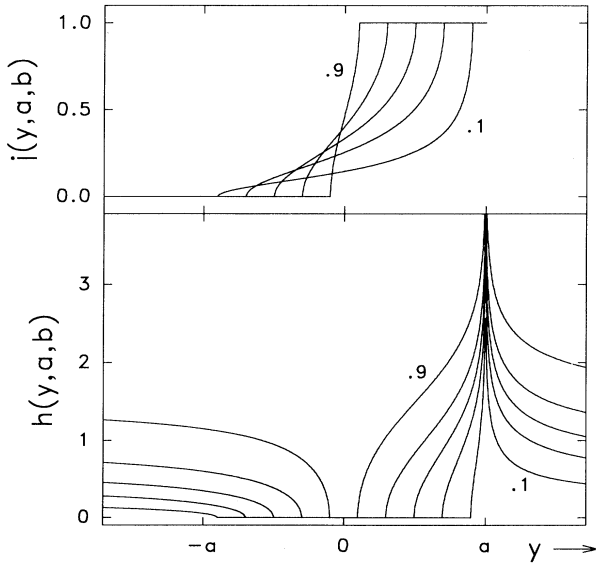


FIG. 6. The universal functions $j(y, a, b)$ (4.3) (top) and $h(y, a, b)$ (4.4) (bottom) for relative penetration depth $(a - b)/a = 0.1, 0.3, 0.5, 0.7, 0.9$.

$$J^*(y) = (J_I + J_H)/2 \;=\; J_c\, j(y,a,b)\ , \tag{4.1}$$

$$H^*(y) = (H_I + H_H)/2 = H_c\, h(y,a,b)\ , \tag{4.2}$$

where

$$j(y,a,b) = \begin{cases} 1, & b \le y \le a \\ \frac{1}{\pi}\operatorname{arccot}\frac{b^2-ay}{p}, & -b \le y \le b \\ 0, & -\infty < y \le -b\ , \end{cases} \tag{4.3}$$

$$h(y,a,b) = \begin{cases} 0, & |y| \le b \\ \frac{y}{2|y|}\operatorname{arctanh}\frac{p}{ay-b^2}, & b \le |y| < \infty\ , \end{cases} \tag{4.4}$$

with $p = [\,|y^2-b^2|\,(a^2-b^2)\,]^{1/2}$. In (4.3) $\operatorname{arccot}x = \pi/2 - \arctan x$ was used rather than $\arctan(1/x)$, which jumps by $\pm\pi$ at $y = b^2/a$. The arctanh in (4.4) applies to both regions $|y| < a$ and $|y| > a$ in contrast to the arctanh in (2.6) and (3.9).

The field (4.2) has an infinity at $y = a$ where $h(y \approx a) = \frac{1}{2}\ln[\,2(a^2-b^2)/b|y-a|\,]$, but no singularity any more at $y = -a$ where $h(y=-a) = \frac{1}{2}\ln(a/b)$. Near $|y| = b$ one has $h \sim (|y|-b)^{1/2}$ and $j - \pi \sim (b-y)^{1/2}$ near $y = b$ and $j \sim (y+b)^{1/2}$ near $y = -b$. For $y \to \pm\infty$ one has $2h = \operatorname{arctanh} c = H_a/H_c$; cf. Eq. (3.6). Due to the weight 1/2 in (4.1, 2) this solution carries half the total current and shields half the applied field of the original solution [cf. (2.5) and (3.5)],

$$I^* = J_c(a^2-b^2)^{1/2}, \quad H_a^* = \frac{H_c}{2}\operatorname{arccosh}(a/b). \tag{4.5}$$

The expressions (4.1)–(4.5) do not describe a real state of the original strip with width $2a$ since any such state requires $|J(y)| = J_c$ at the edges, whereas here $J^*(y) = 0$ for $y < -b$. $J^*$ and $H^*$ rather give the current and field profiles in a strip with width $a+b$ extending from $y = -b$ to $y = a$ for the specific case where at the left edge the width of the region with $|J| = J_c$ has shrunk to zero and thus *no* flux has penetrated there. The applied current and field for this particular case are given by (4.5). For the *larger* ratio $I/H_a$ one has at the left edge $J = +J_c$, and for the *smaller* ratio $J = -J_c$. Expressions (4.1)–(4.4) may also be obtained by integrating $J(y, y_0)$ (2.3) over the interval $b < y < a$.

The property $J^*(-\infty < y < -b) = 0$ allows one to construct new solutions by superimposing appropriately mirror-imaged ($y \to -y$), stretched ($a + b \to 2a$), and shifted ($y \to y \pm y_0$) solutions $J^*$ and $H^*$. The conditions for such superpositions are that their flux-free regions coincide and their current densities vanish outside the strip and take the values $\pm J_c$ at the edges. Furthermore, the history of the applied $I(t)$ and $H_a(t)$ has to be accounted for properly.

As an example we consider the problem where $I$ and $H_a$ are increased from zero such that the flux penetration proceeds monotonically at both edges. Below it will be shown what condition this implies on the path in the $I$-$H_a$ plane. In this case we need the superposition of two of the functions (4.3, 4.4) shown in Fig. 6. Let $J(y) = J_c$ in $b_2 \le y \le a$ and $J(y) = \pm J_c$ in $-a \le y \le -b_1$, and $H(y) = 0$ in the flux-free region $-b_1 < y < b_2$ (Fig. 7). One can show that $|b_2| \le b_1 \le a$ when $I/H_a \ge 0$. Defining the lengths

$$b = \frac{b_1+b_2}{2} \ge 0, \quad w = \frac{b_1-b_2}{2} \ge 0\ , \tag{4.6}$$

one obtains the solution in the form (Fig. 7)

$$J(y) = J_c\,[\,j(y+w, a+w, b) + p\, j(-y-w, a-w, b)\,]\ , \tag{4.7}$$

$$H(y) = H_c\,[\,h(y+w, a+w, b) - p\, h(-y-w, a-w, b)\,]\ , \tag{4.8}$$

with the functions $j$ (4.3) and $h$ (4.4) and $p = \pm 1$; see below. The total current $I$ and applied field $H_a$ of this solution follow from (2.5), (3.5), and (4.5),

$$I = J_c\{[\,(a+w)^2 - b^2\,]^{1/2} + p\,[\,(a-w)^2 - b^2\,]^{1/2}\}\ , \tag{4.9}$$

$$H_a = \frac{H_c}{2}\left[\operatorname{arccosh}\frac{a+w}{b} - p\operatorname{arccosh}\frac{a-w}{b}\right]. \tag{4.10}$$

Note the different signs $+p$ and $-p$ in $J$, $I$ and $H$, $H_a$. For given $I$ and $H_a$ the penetration depths $a - b_1$ and $a - b_2$ are obtained by solving the two coupled transcendental equations (4.9) and (4.10) for $b$ and $w$ to obtain

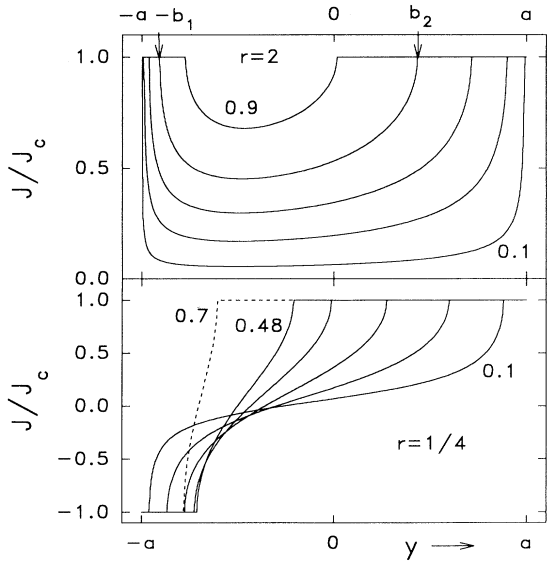


FIG. 7. Current density $J(y)$ (4.7) for a "current-like"(top) and "fieldlike" (bottom) state in a superconducting strip of width $2a$ to which both a transport current $I$ and a magnetic field $H_a$ are applied with constant ratio $r = I/(2\pi a H_a)$. Top: $r = 2$, $I/I_{\max} = 0.1$, 0.3, 0.5, 0.7, 0.9. For $I/I_{\max} = 0.7$, $b_1$ and $b_2$ are indicated by arrows at the top. Bottom: $r = 0.25$, $I/I_{\max} = 0.1$, 0.2, 0.3, 0.4, 0.48; here $b_2$ decreases monotonically; the dashed curve $I/I_{\max} = 0.7$ corresponds to an unphysical case since $b_1$ has passed its minimum and increases again; cf. Eq. (4.34) and text.

$b_1(I,H_a,a) = b + w$ and $b_2(I,H_a,a) = b - w$. Before we give the solution below we have to discuss the sign factor $p = \pm 1$ appearing in (4.6)–(4.10).

From the shape of $j(y,a,b)$ (4.3) it is clear that $J(y)$ (4.7) at the left edge ($y = -a$) takes the value $-J_c$ if $p = -1$ and $+J_c$ if $p = 1$. At the *transition* between these two cases one has $a - w = b$ (or $w = a - b$; in general, $|w| \leq a-b$) and therefore the second terms in (4.6)–(4.10) all vanish. Formally one may thus write $p = 0$. In this particular state one has $b_1 = a$; i.e., the width $a - b_1$ of the current-saturated and flux-penetrated region at the left edge *vanishes*; cf. Fig. 6. With $w = a-b$ inserted one gets from (4.9) and (4.10) the applied current and field in the form $I = I^*(a,b)$ and $H_a = H_a^*(a,b)$. Eliminating $b$ from these two expressions one gets a relation between $H_a$ and $I$ for this special case (remember $H_c = J_c/\pi$, $I_{\max} = 2aJ_c$):

$$H_a = H_a^*(I) = H_c \operatorname{arctanh}(I/I_{\max}) \ , \tag{4.11}$$

$$I = I^*(H_a) \ = \ I_{\max} \tanh(H_a/H_c). \tag{4.12}$$

In the limiting cases this means

$$H_a^*(I) = I/2\pi a, \qquad I \ll I_{\max} \ , \tag{4.13}$$

$$H_a^*(I) = \frac{H_c}{2} \ln \frac{2I_{\max}}{I_{\max} - I}, \quad I \approx I_{\max}. \tag{4.14}$$

From (4.13), which may also be written in the symmetric form $H_a^*/H_c = I/I_{\max}$, one sees that in the two cases $I = I_0$, $H_a = 0$ (with arbitrary $I_0 \ll I_{\max}$) and $I = 0$, $H_a = I_0/(2\pi a) \ll H_c$, the edge singularities in the ideal-shielding states $J_{\text{ideal}}(y)$ (2.1) and (3.1) and $H_{\text{ideal}}(y)$ (2.2) and (3.2) have the *same amplitude*, with same sign at the right edge $y = a$ but *opposite sign at the left edge* $y = -a$. Therefore, if both current and field are increased in such a way that initially $I = 2\pi a H_a$, and in general $I = I^*(H_a) = I_{\max} \tanh(H_a/H_c)$, then the penetration depth at the left edge is zero ($b_1 = a$) and *flux penetrates only from one edge* until full penetration is reached when $I = I_{\max}$.

From these arguments one finds that in (4.6)–(4.10)

$$p = -1, \quad J(y = -a) = -J_c \quad \text{if} \quad I < I^*(H_a) \ ,$$
$$p = +1, \quad J(y = -a) = +J_c \quad \text{if} \quad I > I^*(H_a).$$

This is equivalent to

$$p = -1, \quad H(y = -a) > 0 \quad \text{if} \quad H_a > H_a^*(I) \ ,$$
$$p = +1, \quad H(y = -a) < 0 \quad \text{if} \quad H_a < H_a^*(I).$$

At $y = +a$ one always has $J(y) = J_c$ and $H(y) > 0$.

The two equations (4.9) and (4.10) may be solved analytically by the substitutions

$$\frac{a + w}{b} = \cosh(2u), \quad \frac{a - w}{b} = \cosh(2v) \ , \tag{4.15}$$

$$f = \frac{I}{I_{\max}}, \quad g = \frac{H_a}{H_c}, \quad c = \tanh \frac{H_a}{H_c} \ , \tag{4.16}$$

yielding the symmetric expressions

$$f = \tanh(u + pv), \qquad c = \tanh(u - pv) \ , \tag{4.17}$$

with $p = \operatorname{sgn}(f - c)$. Formally, the sign factor $p = \pm 1$ may be omitted (i.e., put $p = 1$) if one allows for negative $v$, considering the intervalls $-\infty \leq v \leq \infty$, $0 \leq u \leq \infty$. The solution of (4.17) is then

$$u = 2\operatorname{arctanh} f + 2g, \quad v = 2\operatorname{arctanh} f - 2g. \tag{4.18}$$

After some algebra and putting the strip half width $a = 1$, we obtain the desired results

$$b = (1 - f^2)^{1/2}(1 - c^2)^{1/2}, \qquad w = f\,c \ , \tag{4.19}$$

$$b_{1,2} = b \pm w = (1 - f^2)^{1/2}(1 - c^2)^{1/2} \pm f\,c \ , \tag{4.20}$$

with the intervals $-1 \leq b_2 \leq 1$, $|b_2| \leq b_1 \leq 1$, $0 \leq f \leq 1$, $0 \leq c \leq 1$. Formally, by allowing for negative $c$, $-1 \leq c \leq 1$, one has $b_1(c) = b_2(-c)$ and thus both penetration depths are given by the same expression

$$b_i = (1 - f^2)^{1/2}(1 - c^2)^{1/2} \ + \ f\,c \ , \tag{4.21}$$

with $i = 1, 2$. In fact, Eq. (4.21) with definitions (4.16) gives *the general result* for the two penetration depths $1 - b_1$ and $1 - b_2$ *for arbitrary sign of current and field* if one allows for $-1 \leq f \leq 1$, $-1 \leq c \leq 1$. For transparency our discussion will consider *positive* $I$ and $H_a$ only.

Which paths in the $I$-$H_a$ plane yield the required monotonically increasing penetration depths $1 - b_1$ and $1 - b_2$ is easily seen by plotting the lines $b_1 = \text{const}$ and $b_2 = \text{const}$ into *one* plot as shown in Fig. 8 for the $I$-$H_a$ plane. In the $f$-$c$ plane (Fig. 9) these lines are ellipses,

$$f(c, b_i) = |cb_i \pm (1 - c^2)^{1/2}(1 - b_i^2)^{1/2}| \ , \tag{4.22}$$

where $b_i = b_1$ yields the lines $b_2 = \text{const}$ and $b_i = b_2$ the lines $b_1 = \text{const}$. Note the *high symmetry and similarity* of Eqs. (4.20) and (4.22). Substituting

$$f = \quad I/I_{\max} \quad = \sin\alpha \ , \tag{4.23}$$
$$c = \tanh(H_a/H_c) = \sin\beta \ , \tag{4.24}$$

one gets the compact form

$$b_1 = \cos(\alpha - \beta), \quad b_2 = \cos(\alpha + \beta). \tag{4.25}$$

In the $\alpha$-$\beta$ plane (Fig. 10) the lines of constant $b_1$ or $b_2$ are straight lines of slope $\pm 1$. The important line $b_1 = 1$ in these three planes is, respectively, $f = \tanh(g)$ (4.12), $f = c$, or $\alpha = \beta$. This line divides the current-field plane into two regions with "currentlike" and "fieldlike" penetration where at the left edge $J = +J_c$ or $J = -J_c$, respectively.

The allowed paths for nonincreasing $b_1$ and $b_2$ should never cross this line $b_1 = 1$. Some allowed paths are indicated in Fig. 9. They satisfy the conditions

$$db_i = \frac{\partial b_i}{\partial I} dI + \frac{\partial b_i}{\partial H_a} dH_a \leq 0 \tag{4.26}$$

($i = 1, 2$), equivalent to a nondecreasing of both $\alpha - \beta$ and $\alpha + \beta$ because of Eqs. (9)–(11). Obviously, the slope of the allowed paths is limited by the slopes of the lines $b_1 = \text{const}$ and $b_2 = \text{const}$. These slopes in all three planes

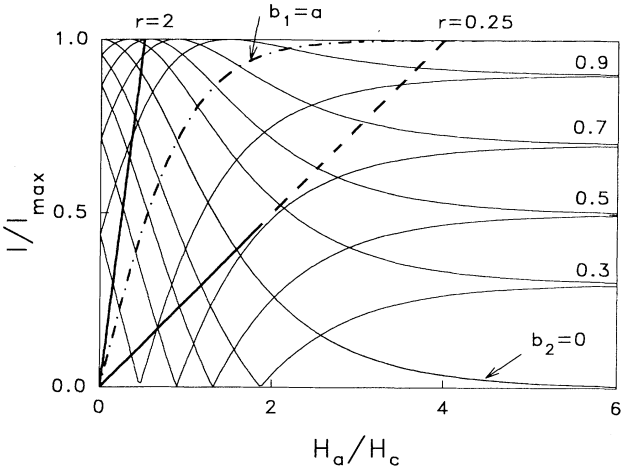


FIG. 8. The lines $b_1 = \text{const}$ (slope $> 0$) and $b_2 = \text{const}$ (slope $< 0$) (4.20) in the $I$-$H_a$ plane. In Figs. 8, 9, and 10 these lines may be identified as follows: The parameters denote $b_1/a$ or $b_2/a$. Whenever a line $b_1 = \text{const}$ touches one of the axes $I = 0$ or $H_a = 0$ this line transforms into a line $b_2 = \text{const}$ with $b_2 = b_1$, and vice versa. Whenever a line $b_1 = \text{const}$ touches the top border $I = I_{\max}$ or the right border $H_a = \infty$, this line transforms into a line $b_2 = \text{const}$ with $b_2 = -b_1$, and vice versa. In Figs. 8, 9, and 10 the dash-dotted line $I/I_{\max} = \tanh(H_a/H_c)$ (or $b_1 = a$) divides the $I$-$H_a$ plane into fieldlike (below) and currentlike (above) regions. In this figure, the straight solid lines are the locus of constant ratio $I/H_a$, namely, $r = (I/H_a)(H_c/I_{\max}) = 2$ and $r = 0.25$. The line $r = 0.25$ is dashed in the unphysical region; see also Fig. 10 and text.

(Figs. 8–10) at all points are *symmetric* about the $x$ and $y$ directions; in the $I$-$H_a$ plane the slopes explicitly are

$$\frac{dH_a}{dI} = \pm S, \quad S = \frac{(I_{\max}^2 - I^2)^{1/2}}{H_c \cosh(H_a/H_c)}. \tag{4.27}$$

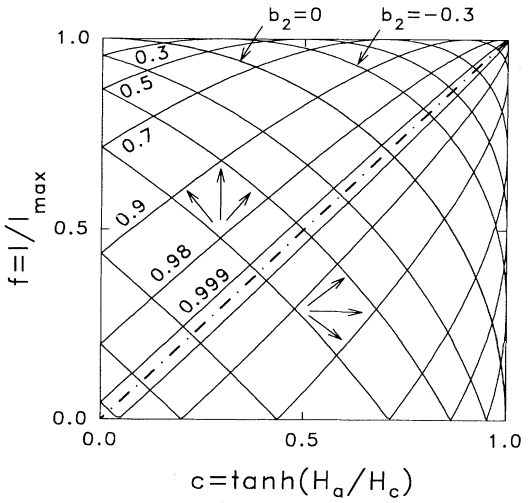


FIG. 9. The lines $b_1 = \text{const}$ (slope $> 0$) and $b_2 = \text{const}$ (slope $< 0$) (4.20) in the $f$-$c$ plane are ellipses. See caption of Fig. 8. The fans of arrows indicate the allowed paths of field and current application.

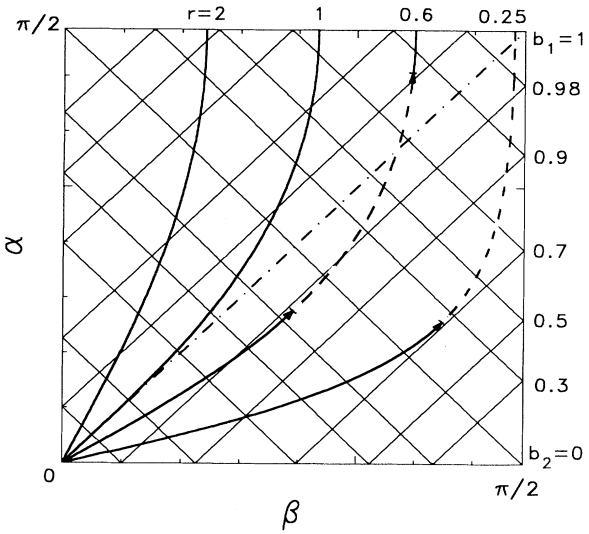


FIG. 10. The lines $b_1 = \text{const}$ (slope $+1$) and $b_2 = \text{const}$ (slope $-1$) (4.20) in the $\alpha$-$\beta$ plane are straight lines. See caption of Fig. 8. The solid lines are loci of constant ratio $r = (I/H_a)(H_c/I_{\max}) = 2$, 1, 0.6, 0.25. The range of unphysical solutions is indicated by the dashed curves; see text.

With the "pure" penetration depths $b_I$ (2.5) and $b_H$ (3.5) for $I = 0$ or $H_a = 0$ inserted, the slope $S$ (4.27) reads

$$S = b_I\, b_H\, I_{\max}/(a^2 H_c) = 2\pi b_I\, b_H\, /a. \tag{4.28}$$

Equation (4.21) or (4.25) reproduces the penetration depths $b_I$, $b_H$, and Eqs. (4.7) and (4.8) the current densities $J_I(y)$ and $J_H(y)$ and fields $H_I(y)$ and $H_H(y)$ of Secs. II and III. Interesting limiting cases in Fig. 9 are

$$f = 0: \quad b_1 = b_2 = (1 - c^2)^{1/2}\ ; \tag{4.29}$$

$$c = 0: \quad b_1 = b_2 = (1 - f^2)^{1/2}\ ; \tag{4.30}$$

$$f = c: \quad b_1 = 1,\ \ b_2 = 1 - 2f^2\ ; \tag{4.31}$$

$$f = 1: \quad b_1 = -b_2 = c\ ; \tag{4.32}$$

$$c = 1: \quad b_1 = -b_2 = f. \tag{4.33}$$

These correspond, respectively, to the cases $I = 0$, $H_a = 0$ (symmetric penetration), $I/I_{\max} = \tanh(H_a/H_c)$ (pure unilateral penetration), and to full currentlike and fieldlike penetration. Note that in the latter two cases the line $y = -b_1 = b_2$ has different meaning: For $f \to 1$ ($I \to I_{\max}$) the line $y = -b_1$ only indicates the position where the Meissner phase has disappeared leaving no trace. But for $c \to 1$ ($H_a/H_c \to \infty$) there remains a trace at $y = -b_1$, namely, a jump of $J(y)$ from $+J_c$ to $-J_c$ and a discontinuity of $H(y)$.

If an experiment is controlled such that during the increase of $I$ and $H_a$ always $f = \tanh g$, i.e., $I = I^*(H_a)$ (4.12), then *no flux penetrates from the left* as stated above and the flux front moves from the right to the left edge. If $I$ and $H_a$ are increased with constant ratio then two cases have to be distinguished: If $I/H_a = \text{const} > 2\pi a$ one has always $p = +1$ and $J(y) = J_c$ at both $y = -a$ and $y = a$. Both penetration depths $a - b_1$ and $a - b_2$ then increase monotonically as $I$ goes from 0 to

$I_{max}$. At $I = I_{max}$ full *asymmetric* penetration is reached with $b_1 = -b_2 = \tanh(H_a/H_c)$ (4.32).

However, if during the increase one has $I/H_a = \text{const} < 2\pi a$ then the path in the $I$-$H_a$ plane crosses the line $f = \tanh g$; there, $p$ changes from $-1$ to $+1$, and $J$ at the left edge jumps from $-J_c$ to $J_c$, when $I$ passes through the value $I^*(H_a)$ (4.12). In this case the penetration depth $a - b_1$ (4.20) or (4.25) at the left edge first increases, reaches a maximum, and then decreases again, reaching zero when $I = I^*(H_a)$, and then increases again. For a given ratio $r = f/g = I/(2\pi a H_a) < 1$ this minimum of $b_1$ occurs at a value $b_m(r)$ which is obtained by solving the transcendental equation

$$g^2 + \cosh^2 g = 1/r^2 \tag{4.34}$$

and inserting the resulting $g = g_m = H_{a,m}/H_c$ into

$$b_m = r + r\, g \tanh g \tag{4.35}$$

(if $a = 1$). This yields $H_a = H_{a,m} = g_m H_c$ and $b_1 = a b_m$ with limiting cases

$$g_m = \ln(2/r), \quad b_m = r\ln(2e/r), \quad r \ll 1\ , \tag{4.36}$$

$$g_m = (1-r)^{1/2}, \quad b_m = 1 - (1-r)^2/2, \quad r \approx 1. \tag{4.37}$$

During the decrease of $a - b_1$ flux has to *exit*. However, this is not possible reversibly due to pinning. As a consequence, flux with opposite sign enters at the left edge and annihilates the frozen flux similarly as shown in Figs. 2 and 4. When this new flux front meets the frozen flux front then the penetration depth $a - b_1$ starts to increase again and the solution (4.7)–(4.10) is again valid. Therefore, after $b_1$ has reached its minimum value $b_m$ (4.35), the real current and field profiles look different from those given by Eqs. (4.7) and (4.8) until $b_1$ has reached $b_m$ again. For small values of $r$ this reentrant behavior does not occur; see the cases $r = 0.6$ and $r = 0.25$ in Fig. 10.

If $I(t)$ and $H_a(t)$ are increased such that the penetration depths $a - b_1$ and $a - b_2$, obtained from (4.9) and (4.10) do not increase monotonically, or if $I(t)$ and $H_a(t)$ are cycled, then the field and current profiles of the strip are linear superpositions of more than two functions of the type (4.3), (4.4). These profiles look smilar to those of Eqs. (2.11), (2.12), and (3.20), (3.21), but in general are more complex. In particular, it may happen that $J(y)$ gets cusps or even hits the value $J_c$ at an isolated point away from the edges. The discussion of such particular histories of $I(t)$ and $H_a(t)$ and a general numerical program will be published elsewhere.

## V. DOUBLE STRIPS AND RINGS IN A PERPENDICULAR FIELD

In this section we discuss the field and current profiles in a double strip closed at its ends, and in a flat superconducting ring, and in combinations thereof, when a perpendicular field is applied (Fig. 11). This field $H_a$ induces a circulating current $I$ which shields the interior of the loop such that the total magnetic flux through it is zero. At the same time, the local field $H_a'$ at the position of the strips is partly shielded from the interior of the strip. The field $H_a'$ exceeds $H_a$ by the field caused by the current $I$ flowing in the neighboring strip. If $I < I^*(H_a') = I_{max}\tanh(H_a'/H_c)$ (4.12) then the currents at the two edges of the strip flow in opposite directions and flux of the same orientation enters at the two edges. If $I = I^*(H_a')$ the shielding current along the inner edge is zero and flux penetrates the strip only from the outer edge. If $I > I^*(H_a')$ the current flows in the same direction throughout the strip, and flux of opposite sign penetrates from the two edges. We shall now discuss how these different situations may be realized.

The transport current $I$ induced by an applied field $H_a$ in a long double strip connected at its ends, in principle, can be calculated *exactly* by conformal mapping. We shall use here a more transparent method to estimate the circulating current and the field at the strip. We assume that the distance $2R$ between the centers of the two strips, or the diameter $2R$ of a circular ring, is much larger than the width $2a$ of the strips. Any closed loop formed by the superconducting strip shields an applied field from its interior. Thus the flux $\Phi$ of the applied field inside the loop is exactly compensated by the flux caused by the circulating supercurrent $I$. From the area $A$ and the inductivity $L$ of the loop one obtains $I = \Phi/L = \mu_0 H_a A/L$. For a closed double strip of length $l$ and for the ring one has[37]

$$A = 2(R-a)l, \quad L \approx (\mu_0 l/\pi)\ln(2R/a) \quad \text{(double strip)}\ ,$$

$$A = \pi(R-a)^2, \quad L \approx \mu_0 R\,[\ln(8R/a) - 2] \quad \text{(ring)}.$$

We have omitted here the contribution to the inductivities $L$ which is caused by the field inside the conductors since the strip thickness is $d \ll a$. The circulating current then becomes

$$I \approx 2\pi(R-a)H_a/\ln(2R/a) \quad \text{(double strip)}\ , \tag{5.1}$$

$$I \approx \pi(R-a)^2 H_a/R\ln(R/a) \quad \text{(ring)}. \tag{5.2}$$

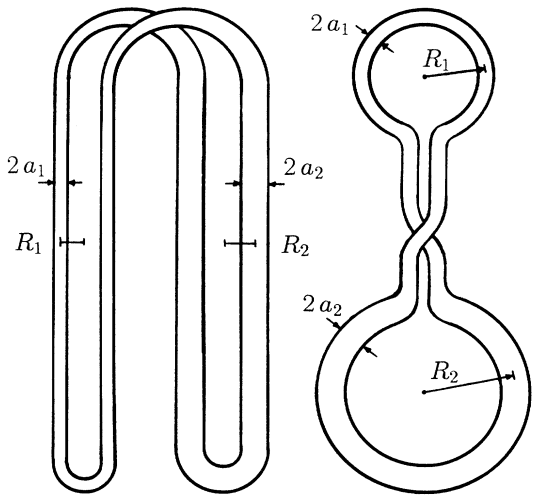


FIG. 11. Two suggested configurations of asymmetric double loops of superconducting films. By appropriate choice of the widths $2a$ and distances $2R$ the flux penetration into the strip becomes fieldlike or currentlike; see text.

For the double strip the external field $H_a$ at each strip may be approximated by the applied field plus the field caused at the center of this strip by the current through the other strip at distance $2R$,

$$H_a' = H_a + \frac{I}{4\pi R} = H_a\left[1 + \frac{1 - a/R}{2\ln(2R/a)}\right]. \tag{5.3}$$

From (5.1)–(5.3) we obtain that the ratio $r = I/(2\pi a H_a') = 1$ if $R/a \approx 3.4$ for the double strip and if $R/a \approx 5$ for the ring. These estimates are crude since in the derivation of (5.1)–(5.3) $R \gg a$ was assumed. A better estimate for the double strip is obtained by calculating the total flux between the strips from the Meissner fields (2.2) and (3.2) and equating this to zero. This yields a smaller ratio $I/H_a'$ and gives $r = 1$ for $R/a \approx 5.5$. For smaller $R/a$ the flux penetration into the strip is initially fieldlike ($r < 1$), and for larger $R/a$ it is currentlike ($r > 1$).

The condition $r = 1$ means that initially (for $H_a \ll H_c = J_c/\pi$) no flux enters at the inner edge since $I = I^*(H_a') \approx H_a'/(2\pi a)$. If $H_a$ is increased, then, even for an initially small ratio $r < 1$, the induced current $I \sim H_a$ eventually will exceed the value $I^*(H_a')$ since this saturates to $I_{\max} = 2aJ_c$. Flux with opposite orientation will then enter from both edges as discussed in Sec. IV.

The interesting low-current situation $r < 1$ can be realized in various ways by modifying the geometry. Obviously, if the loop is interrupted then $I = 0$ and the strip behaves as described in Sec. III. The opposite case $r \gg 1$ is achieved by choosing $R \gg a$; then $I > I^*$ always holds. The induced current can be reduced by connecting two loops such that the current in these circulates *in opposite directions* (Fig. 11). In a double ring with the shape of a symmetric 8 the transport current $I$ induced by a homogeneous field $H_a$ is exactly zero. In general, two well separated rings with radii $R_1$, $R_2$ and strip widths $a_1$, $a_2$ connected in phase (+) or in antiphase (−) exhibit an induced transport current

$$I \approx \pi H_a \frac{(R_1 - a_1)^2 \pm (R_2 - a_2)^2}{R_1 \ln(R_1/a_1) + R_2 \ln(R_2/a_2)}. \tag{5.4}$$

Similarly, two loops of a double strip of lengths $l_1$, $l_2$, separations $2R_1$, $2R_2$, and widths $a_1$, $a_2$ exhibit a current

$$I \approx 2\pi H_a \frac{(R_1 - a_1)\, l_1 \pm (R_2 - a_2)\, l_2}{l_1 \ln(2R_1/a_1) + l_2 \ln(2R_2/a_2)}. \tag{5.5}$$

Thus, any desired ratio $I/H_a$ can be achieved by choosing the size and shape of a double loop appropriately. Combining this with a suitable increase and decrease of $H_a(t)$ one achieves a rich variety of field profiles which may be observed by magneto-optics or with Hall probes.

Note that for $r < 1$ the field $H$ near the strip edge inside the loop varies nonmonotonically (has three extrema). This is easily seen by adding the two ideal shielding fields outside a strip, the $\approx$ monopolar field $H_I(y)$ (2.2) and the $\approx$ dipolar field $H_H(y)$ (3.2), yielding

$$H_I + H_H = 2H_a(y - ra)/(y^2 - a^2)^{1/2}\ , \tag{5.6}$$

which has a minimum if $r < 1$.

## VI. CONCLUSIONS

The obtained results have important consequences. The most spectacular feature, which was often seen in experiments, is that perpendicular flux penetrates into flat samples *delayed* as if there were a surface barrier or an unphysically large $H_{c1}$: The penetration depth increases first slowly, $a - b \sim H_a^2$, and then almost linearly (Fig. 12). This was shown for the first time experimentally and theoretically in Ref. 38, where flux penetration into a thin strip was computed numerically. Extrapolating the penetration depth $a - b(H_a)$ (3.5) in Fig. 12 by a straight line through the inflection point we may define a pseudo first critical field

$$H_p = H_c[\mathrm{arcsinh}(1) + 2^{1/2} - 2] \approx 0.296 H_c. \tag{6.1}$$

If $j_c$ is high this penetration field $H_p$ exceeds the thermodynamic penetration field $\approx H_{c1}d/a$ by far. Thus, numerous measurements which for perpendicular $H_a$ show an upturn of $H_{c1}(T)$ at low temperatures (where also $j_c$ greatly increases; for references see Ref. 39) can be interpreted in terms of flux penetration controlled simply by constant volume pinning as calculated in our model.

Moreover, the above obtained cubic deviation of the magnetic moment from the ideal screening value $\delta M = M - \pi a^2 H_a \sim H_a^3$ explains, without the assumption of a surface barrier, why the "cubic fit" of $\delta M(H_a)$ proposed by Burlachkov *et al.*[39] to get the expected BCS temperature dependence of $H_{c1}$ works so well. We think that models of a surface barrier are *not* required in this case and all experimental data can be described in a natural way by the critical-state model. In addition, a wrong interpretation of the penetration field $H_p$ as the lower critical field $H_{c1} \sim \lambda^{-2}$ in perpendicular geometry gives a too small value of the London penetration depth $\lambda$ or $\lambda_{ab}$ in $c$-oriented high-temperature superconductors.

The slow initial penetration of the magnetic flux $\Phi \sim H_a^2$ can be explained by reconsidering the process of current saturation near the strip edges as shown in Fig. 13. The depth where the ideal screening current (3.2) exceeds $J_c$ and the current saturates is $\delta_{\rm est} \approx 2aH_a^2/J_c^2$ at $H_a \ll J_c$. This estimate is smaller by a factor $\pi^2/4 \approx 2.5$ than our precise analytical value $a - b = aH_a^2/2H_c^2$ and

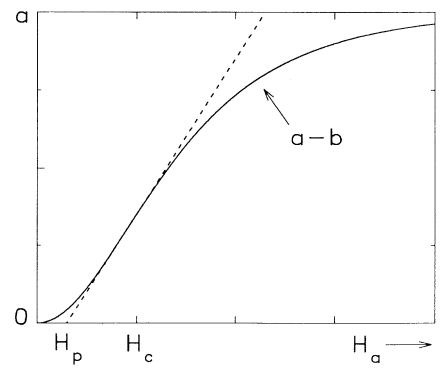


FIG. 12. The penetration depth $a - b$ (3.5) of a magnetic field $H_a$ applied perpendicular to a strip of width $2a$. The dashed line through the inflection point defines the penetration field $H_p$.

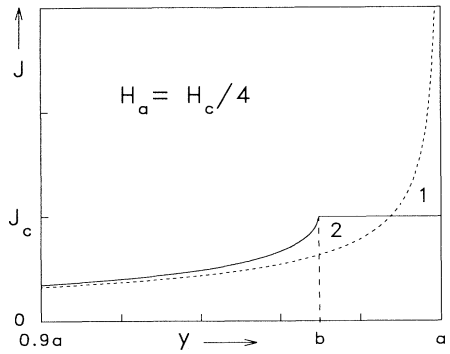


FIG. 13. The saturation of the current density $J(y)$ near the edge of the strip. The dashed curve gives the ideal $J(y)$ (3.1) [or (3.7) with $b = a$]. The solid line gives $J(y)$ (3.7) for $H_a = H_c/4$ where $b \approx 0.97a$. Area 1 ($\sim H_a^2$) approximately equals area 2; the difference of these areas is $\approx \delta M/(2a^2) \sim H_a^3$.

should not be used in quantitative calculations as was done, e.g., in Ref. 40. The physical reason for this deeper penetration is a redistribution of the currents after cutting off the area 1 in Fig. 13: In order to compensate for the decreased screening, more current (area 2 in Fig. 13) has to be added in the Meissner region. The magnetic moments of these two areas nearly compensate. Therefore, the simple cutoff gives a too large decrease of the magnetization with a wrong $H_a$ dependence $\delta M_{\rm est} \sim H_a^2$ instead of the correct $\delta M \sim H_a^3$.

The slow flux penetration $a - b \sim H_a^2$ or $\sim I^2$, $\delta M \sim H_a^3$ and the extremely small losses $P \sim H_a^4$ or $\sim I^4$ result only for the assumed *constant thickness* $d$. For ellipsoidal specimen cross section one has $d(y) \sim (a^2 - y^2)^{1/2}$ and thus a spatially varying critical sheet current $J_c(y) = j_c d(y) \sim (a - |y|)^{1/2}$ near the edges. In this case one obtains *faster* penetration of flux, namely, $a - b \sim H_a$ or $\sim I$, $\delta M \sim H_a^2$, and $P \sim H_a^3$ or $\sim I^3$, *like in the original Bean model.* This conclusion for ellipsoids follows from similar arguments as given in connection with Fig. 13; see also Norris[22] for applied current, and the computations[41] for an applied field. Exact results for varying $J(y)$ may be obtained along the lines of this paper, e.g., by introducing a weight factor $J(y)/J(0)$ in the integral (3.4). It is our belief that the rectangular cross section treated in our paper is relevant to most experiments on superconducting single crystals and films.

The delayed flux penetration is very important for the proper function of superconducting quantum interference devices (SQUID's). The flux concentration[40] decreases with the onset of flux penetration at $H_a > H_p = 0.0941 j_c d$ and the response to the magnetic field becomes *nonlinear.* Above $H_p$ the presence of Abrikosov flux lines causes *additional noise.* High $j_c$ is, therefore, a key requirement for SQUID's that is not mentioned usually.

A further, seemingly contradictory feature of perpendicular geometry occurs when $I$ or $H_a$ is reversed or cycled. As can be seen in Figs. 2 and 4, there is a region immediately inside the outer flux front (at $|y| = b'$) where $J(y)$ has reversed its sign but $\nabla B$ has not yet. In this region the driving force on the flux lines is thus opposed to the force exerted by the flux-density gradient. Since here $|J| < J_c$, this uphill motion of the flux lines can occur only as flux creep, which is not considered in our paper. However, for particular magnetic and current histories such an uphill motion of flux lines against the flux-density gradient really *does* occur since $J(y)$ reaches $J_c$ at an isolated point away from the edges. This unexpected behavior can be realized even with a monotonically changing field, without applying a current, if the critical current density is nonuniform, $J_c = J_c(y)$. Work on these interesting situations is in progress.

The finding of flux drift *against* the flux-density gradient clearly contradicts the original critical-state model for longitudinal geometry. This seeming paradox is resolved as follows for thick and thin films: If $d \gg \lambda$, our model considers only the projection of the current-induced classical Bean critical state across the $x$ direction. If $d < \lambda$, this longitudinal Bean state is absent, but the vortices are now nearly perpendicular to the surface and the driving force exerted on the flux lines by the flux-density gradient is negligibly small since the driving current is a Meissner current. In both cases, the general statement holds that for $d \ll a$ the current is predominantly caused by the *transversal* gradient $\partial H_y/\partial x$, causing also the curvature of field lines if $H_x \neq 0$, and not by the flux-density gradient $\partial H_x/\partial y$ (Sec. I).

In conclusion, in flat type-II superconductors with thickness $d \to 0$ and critical current density $j_c$ =const, when a transport current or a perpendicular magnetic field, or both, are applied, the penetrating flux front and also the jump of the current density have *vertical slope* and the current density is *finite* everywhere. A weak logarithmic singularity of the field occurs at the edges, $|H| \sim \ln|a - |y||$, which for $j_c \to \infty$ or $I \ll I_{\rm max} = 2aJ_c$ or $H_a \ll H_c J_c/\pi$ becomes stronger, $|H| \sim |a - |y||^{-1/2}$. Finite $d$ smears these singularities over a width $\approx d$. As soon as the current and the applied field are reduced, *the sheet current falls below $J_c$ everywhere* (Figs. 2 and 4). In thin films this means that the current density $j = J/d$ also falls below $j_c$, and thus the relaxation comes to a halt. Such an effect was experimentally observed and explained recently.[42] In thick samples ($d \gg \lambda$) the sheet current $J = (h_+ - h_-)j_c$ will continuously relax as usual in a classical Bean critical-state with Anderson's relaxation of $j_c$, but this relaxation comes from flux motion *perpendicular* to the specimen. During reversal of the applied field or current, the penetrating reversed current density drives the flux lines "uphill" against the flux-density gradient.

All these analytical results are in contrast to the widely used Bean critical-state model for longitudinal fields. However, Bean's main assumption that the flux lines start to move only when $j$ reaches $j_c$ works very well also in perpendicular geometry; this is confirmed by comparing the theoretical penetration depth (3.5) and field profiles (3.9) with experiments,[38] and by direct measurements of the current distribution in the critical state.[43]

## ACKNOWLEDGMENT

M. V. Indenbom thanks the Alexander von Humboldt Foundation for support.

*Permanent address: Institute of Solid State Physics, 142432 Chernogolovka, Russia.
[1]J. G. Bednorz and K. A. Müller, Z. Phys. B **64**, 189 (1986).
[2]M. K. Wu, J. R. Ashburn, C. J. Torng, P. H. Hor, R. L. Meng, L. Gao, Z. J. Huang, Y. Q. Wang, and C. W. Chu, Phys. Rev. Lett. **58**, 908 (1987).
[3]A. M. Campbell and J. Evetts, Adv. Phys. **21**, 199 (1972).
[4]S. Senoussi, J. Phys. (France) III **2**, 1041 (1992).
[5]T. K. Worthington, M. P. A. Fisher, D. A. Huse, J. Toner, A. D. Marwick, T. Zabel, C. A. Feild, and F. Holtzberg, Phys. Rev. B **46**, 11854 (1992).
[6]E. Sandvold and C. Rossel, Physica C **190**, 309 (1992).
[7]Ph. Seng, R. Gross, U. Baier, M. Rupp, D. Koelle, R. P. Huebener, P. Schmitt, G. Saemann-Ischenko, and L. Schultz, Physica C **192**, 403 (1992).
[8]J. C. van der Beek, G. J. Nieuwenhuys, P. Kes, H. G. Schnack, and R. P. Griessen, Physica C **197**, 320 (1992).
[9]H. Theuss, A. Forkl, and H. Kronmüller, Physica C **190**, 345 (1992).
[10]Th. Schuster, M. R. Koblischka, B. Ludescher, N. Moser, and H. Kronmüller, Cryogenics **31**, 269 (1991).
[11]L. A. Dorosinskii, M. V. Indenbom, V. I. Nikitenko, Yu. A. Ossip'yan, A. A. Polyanskii, and V. K. Vlasko-Vlasov, Physica C **203**, 149 (1992).
[12]P. Brüll, D. Kirchgässner, and P. Leiderer, Physica C **195**, 157 (1991).
[13]A. A. Abrikosov, *Fundamentals of the Theory of Metals* (North Holland, Amsterdam, 1988); E. H. Brandt and U. Essmann, Phys. Status Solidi B **144**, 13 (1987).
[14]E. H. Brandt, Physica B **169**, 91 (1991); Int. J. Mod. Phys. B **5**, 751 (1991).
[15]E. H. Brandt, Physica C **195**, 1 (1992).
[16]M. V. Feigel'man, V. B. Geshkenbein, A. I. Larkin, and V. M. Vinokur, Phys. Rev. Lett. **63**, 2303 (1989).
[17]G. Blatter and V. B. Geshkenbein, Phys. Rev. B **47**, 2725 (1993); G. Blatter, M. V. Feigel'man, V. B. Geshkenbein, A. I. Larkin, and V. M. Vinokur, Rev. Mod. Phys. (to be published).
[18]C. P. Bean, Rev. Mod. Phys. **36**, 31 (1964); J. Appl. Phys. **41**, 2482 (1970).
[19]D. J. Frankel, J. Appl. Phys. **50**, 5402 (1979).
[20]M. Daeumling and D. C. Larbalestier, Phys. Rev. B **40**, 9350 (1989).
[21]L. W. Connor and A. P. Malozemoff, Phys. Rev. B **43**, 402 (1991).
[22]W. T. Norris, J. Phys. D **3**, 489 (1970); see also G. W. Swan, J. Math. Phys. **9**, 1308 (1968); A. I. Larkin and Yu. N. Ovchinnikov, Zh. Eksp. Teor. Fiz. **62**, 1231 (1972) [Sov. Phys. JETP **34**, 651 (1972)].
[23]P. N. Mikheenko and Yu. E. Kuzovlev, Physica C **204**, 229 (1993); see also J. Zhu, J. Mester, J. Lockhart, and J. Turneaure, *ibid.* **212**, 216 (1993).
[24]E. H. Brandt, M. Indenbom, and A. Forkl, Europhys. Lett. **22**, 735 (1993).
[25]E. H. Brandt, Phys. Rev. B **48**, 6699 (1993).
[26]E. H. Brandt and M. Indenbom (unpublished).
[27]L. Civale, A. D. Marwick, T. K. Worthington, M. A. Kirk, J. R. Thompson, L. Krusin-Elbaum, Y. Sun, J. R. Clem, and F. Holtzberg, Phys. Rev. Lett. **67**, 648 (1991).
[28]W. Gerhäuser, G. Ries, H. W. Neumüller, W. Schmidt, O. Eibl, G. Saemann-Ischenko, and S. Klaumünzer, Phys. Rev. Lett. **68**, 879 (1992).
[29]D. R. Nelson and V. M. Vinokur, Phys. Rev. Lett. **68**, 2398 (1992); E. H. Brandt, *ibid.* **69**, 1105 (1992); Europhys. Lett. **18**, 635 (1992); I. F. Lyuksyutov, *ibid.* **20**, 273 (1992).
[30]W. K. Kwok, U. Welp, G. W. Crabtree, K. G. Vandervoort, R. Hulscher, and J. Z. Liu, Phys. Rev. Lett. **64**, 966 (1990); B. M. Lairson, S. K. Streiffer, and J. C. Bravman, Phys. Rev. B **42**, 10067 (1990).
[31]M. Kulić and F. Rys, J. Low Temp. Phys. **76**, 167 (1989).
[32]G. Blatter, J. Rhyner, and V. M. Vinokur, Phys. Rev. B **43**, 7826 (1991).
[33]E. H. Brandt, Phys. Rev. B **46**, 8628 (1992).
[34]J. R. Clem, R. P. Huebener, and D. E. Gallus, J. Low Temp. Phys. **12**, 449 (1973).
[35]E. H. Brandt, Z. Phys. B **80**, 167 (1990).
[36]E. H. Brandt, P. Esquinazi, H. Neckel, and G. Weiss, Phys. Rev. Lett. **56**, 89 (1986); J. Low Temp. Phys. **63**, 187 (1986); E. H. Brandt, J. Phys. (Paris) Colloq. **48**, C831 (1987).
[37]L. D. Landau and E. M. Lifshitz, *Electrodynamics of Continuous Media*, Vol. VIII: Theoretical Physics (Pergamon, Oxford, 1963).
[38]M. V. Indenbom, A. Forkl, H.-U. Habermeier, and H. Kronmüller, J. Alloys Compounds **195**, 499 (1993).
[39]L. Burlachkov, Y. Yeshurun, M. Konczykowski, and F. Holtzberg, Phys. Rev. B **45**, 8193 (1992).
[40]E. Aharoni, G. Koren, Cohen Daniel, and Cohen David, Physica C **202**, 263 (1992).
[41]V. M. Krasnov, V. A. Larkin, and V. V. Ryazanov, Physica C **174**, 440 (1991).
[42]M. Darwin, J. Deak, L. Hou, M. McElfresh, E. Zeldov, J. R. Clem, and M. Indenbom, this issue, Phys. Rev. B **48**, 13 192 (1993).
[43]V. K. Vlasko-Vlasov, L. A. Dorosinsky, M. V. Indenbom, V. I. Nikitenko, A. A. Polyansky, and R. L. Prozorov, Superconductivity: Physics, Chemistry, Technics **6**, No. 4, (1993).